Temperature dependence of Raman scattering in stabilized cubic zirconia

Jiguang Cai, Constantine Raptis, Yannis S. Raptis, and Evangelos Anastassakis
Department of Physics, National Technical University, Athens 15780, Greece
(Received 22 July 1994)

The temperature dependence of Raman spectra of cubic yttria-stabilized zirconia (YSZ) for three yttria concentrations (10, 15, and 20 wt %) is investigated in the range 40–1470 K. The variation of the spectra with temperature implies that first-order scattering (one-phonon processes) is dominant in this material, providing further evidence that the broad features observed in the spectra are caused mainly by partial lattice disorder rather than by combination (higher-order) processes. The high-temperature phase of YSZ is entirely stable in this range and remains cubic throughout. The temperature-induced frequency shifts of the band at $\sim 600\ \mathrm{cm}^{-1}$ (attributed to the F_{2g} zone-center optic mode) are determined for the three different yttria concentrations. Furthermore, using uniaxial stress data as well, the volume contribution to such shifts is calculated and compared to the lattice anharmonicity contribution. It is found that the volume contribution is larger than the total effect (by a factor of about 2) for all three compositions at 300 K, implying that the bonding in cubic YSZ has ionic character.

I. INTRODUCTION

At atmospheric pressure, pure zirconia (ZrO_2) has three structures between room temperature (RT) and its melting point at 3100 K,[1–5] i.e., monoclinic structure (space group C_{2h}^5) from RT up to a temperature (T) in the range 1225–1450 K, tetragonal structure (D_{4h}^{15}) between 1425 and ~2650 K, and cubic fluorite structure (O_h^5) for $T > 2650$ K. The cubic fluorite structure of zirconia can be also stabilized by a variety of divalent or trivalent metal oxides and rare-earth oxides from RT up to 2770 K.[6,7] One of these stabilizers is yttria (Y_2O_3).

The yttria-stabilized zirconia (YSZ) crystals have disordered cubic face-centered fluorite-type lattices in which the tetravalent Zr^{+4} cations are partially substituted by the trivalent Y^{+3} cations and one oxygen vacancy per pair of Y^{+3} ions is generated in some cubic zirconia elementary cells. Hence, YSZ is well known as a high-temperature material and a good oxygen-ion conductor, and has many applications in optical and electronic technologies.

It is well known that a number of physical properties of materials depend on the interactions between vibrational modes of atoms, molecules, ions or lattices. In order to obtain the information on such interactions in solids, it is necessary to investigate the way the lattice vibration frequencies vary with temperature. A large number of solids have been studied in this way, using spectroscopic methods, e.g., diamond,[8,9] Si (Ge),[10–12] ZnSe,[13] MF_2 (M=Ca, Sr, Ba),[14] Mg_2X (X=Si, Ge, Sn),[15] AlSb,[16] α-$LiIO_3$,[17] LaF_3,[18] etc.

In this work, we present Raman-scattering measurements from cubic YSZ crystals under variable temperature (40–1470 K) for three yttria contents (10, 15, and 20 wt %) with emphasis being given to the T dependence of the F_{2g} Raman mode at $\sim 600\ \mathrm{cm}^{-1}$. The experimental data on the T dependence of the phonon frequencies of this work in combination with previously reported uniaxial stress data are analyzed, and shown to consist of two parts: the volume effect (implicit effect) and the lattice anharmonicity effect (pure temperature effect or explicit effect).

II. EXPERIMENTAL SETUP

The samples of cubic YSZ crystals were polished transparent rectangular rods ($1.5 \times 1.5 \times 15\ \mathrm{mm}^3$), oriented along $(x,y,z)=([100],[010],[001])$. Most spectra were obtained using the $y(xy)x$ light-scattering configuration, where the first (last) letter indicates the direction of the incident (scattered) light and the first (last) letter in parentheses refers to the direction of polarization of the incident (scattered) light.

The experimental setup for obtaining the Raman spectra under variable T is shown schematically in Fig. 1. Low-temperature measurements (40–300 K) were performed with the samples inside a liquid-helium closed-cycle cryostat (Cryogenics Technology); the accuracy of T measurements was ±2 K.

For the high-temperature experiments (300–1473 K), the samples were placed inside a fused silica cell which, in its turn, was inserted in a vacuum-operated water-cooled resistance (molybdenum or tungsten wire) furnace.[20] The temperature was determined by a pair of Chromel-Alumel thermocouples attached appropriately to a flexible seath which allowed precise positioning of the thermocouples relative to the sample. For temperatures up to 1300 K, the T measurements were direct, with one of the thermocouples placed close to the sample holder (silica cell); using this arrangement, the T accuracy was estimated to be ±3 K. Given that the limit for continuous operation of these thermocouples is ~1300 K, T measurements above this limit were carried out as follows: one thermocouple was positioned close to the sample holder while the second was placed away from it (out-

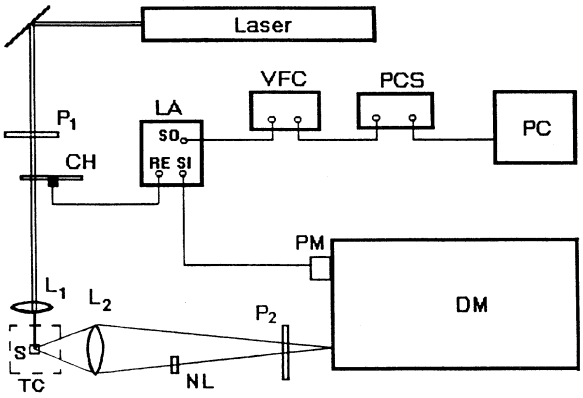

FIG. 1. Schematic diagram of the experimental setup used for variable temperature Raman scattering (90° geometry). P_1, P_2: polarizers; L_1, L_2: lenses; CH: chopper; S: sample; TC (temperature controller): liquid-helium closed-cycle cryostat or water-cooled resistance furnace; NL: neon calibration lamp; DM: double monochromator; PM: photomultiplier; LA: lock-in amplifier; (RF): reference frequency; SI: signal input, SO: signal output); VFC: voltage-to-frequency converter; PCS: photon counting system; PC: PC computer for data handling.

side the radiation shields, see Ref. 20), so that two simultaneous readings could be obtained. The two sets of readings were found to relate almost linearly. Therefore, by measuring the T outside the radiation shields, it was possible to estimate the T close to the sample. Bearing in mind that the temperatures measured outside the shields were much lower than the corresponding ones near the sample, it became possible to extend the range of T measurements up to 1600 K by extrapolating the linear relation between the two sets of T readings; the T accuracy in this case was estimated to be ± 5 K.

The Raman measurements were performed with the 496.5, 488.0, and 457.9 nm lines of an Ar^+ laser, at a power level of ~ 100 mW. The 457.9-nm line was used for experiments at very high temperatures, because the background level due to blackbody radiation from the sample and the hot parts of the cell was lower in the spectral region around this line, while in the vicinity of the green line at 496.5 nm, this thermal background was very intense for temperature above 1200 K. At very high temperatures (>1300 K), the laser chopping technique was also used to check and eventually reduce the level of the thermal radiation. Using this technique and the green line for the excitation it was possible to match, but not exceed, the level of the signal-to-noise ratio obtained by employing the deep blue laser line alone; consequently, we performed most of the high-T measurements using the latter line, without any chopping. The scattered light was detected at 90°, as described in Ref. 19, except that the four slits of the spectrometer were set at 250, 300, 300, and 250 μm for $T<1100$ K and reduced to 200, 240, 240, and 200 μm at $T>1100$ K. The entrance slit height was set at 10 mm throughout.

III. EXPERIMENTAL RESULTS

The room-temperature $y(xy)x$ Raman spectra of cubic YSZ for the three concentrations are shown in Fig. 2, excited by the 496.5-nm Ar^+ laser line. Only F_{2g} symmetry species are present in the Raman spectra of this configuration. The dominant feature of these spectra is the intense peak at ~ 600 cm^{-1} which is further discussed below. Figure 3 shows the $y(zz)x$ spectrum (corresponding to $A_{1g}+4E_g$ symmetry species) of 15 wt. % YSZ and, for comparison, the corresponding $y(xy)x$ spectrum of the same concentration using the same intensity scale. Figure 4 illustrates the Raman spectra of 15 wt. % YSZ excited by the 496.5-nm line at temperatures 40, 300, and 1173 K (the sharp line is the Ne calibration line). Figure 5 shows the Raman spectrum of 20 wt. % YSZ at various temperatures up to 1473 K excited by the 457.9-nm line. In order to compare the data obtained with and without the laser chopping technique, we show in Figs. 6(a) (without chopping) and 6(b) (with chopping) the corresponding spectra of 20 wt. % YSZ at $T=300$ and 1273 K, again using the 457.9-nm line for the excitation. As can be seen, there is not much difference between the two sets of data, thus confirming that, for experiments up to this temperature, the level of the blackbody radiation is negligible in the vicinity of the deep blue line. Whether the chopping technique was used or not, reliable observation of the Raman band at ~ 600 cm^{-1} was possible up to 1373 K for the 20 wt. % sample, and up to 1273 K for the 10 and 15 wt. % samples.

The method for determining the temperature-induced phonon frequency shifts of the rather broad F_{2g} band have been described previously.[19] Plots of phonon frequencies against T are shown in Fig. 7 for all three concentrations and, for later use, these results are fitted by a polynomial function (solid lines in Fig. 7) of the form

$$\omega(T)=\omega(0)+a_1T+a_2T^2\,, \tag{1}$$

where T is in units of K. The fitting values $\omega(0)$, a_1, and a_2 are given in Table I.

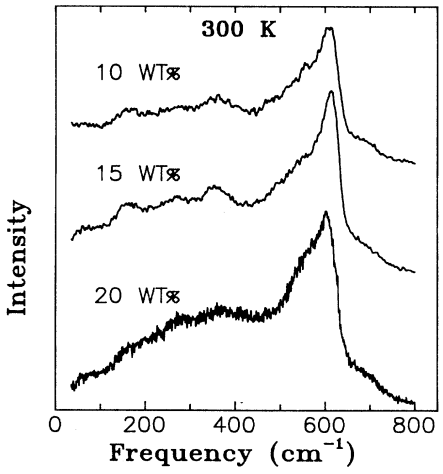

FIG. 2. Typical $y(xy)x$ Raman spectra of cubic YSZ at 300 K for the 10, 15, and 20 wt. % compositions corresponding to the F_{2g} symmetry and excited by the 496.5-nm Ar^+ laser line.

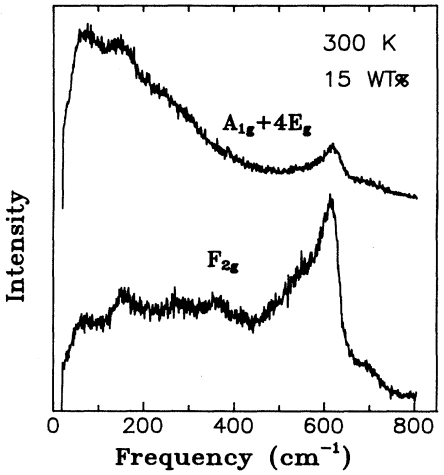

FIG. 3. Room-temperature $y(zz)x$ (upper spectrum) and $y(xy)x$ (lower spectrum) Raman spectra of 15 wt. % YSZ excited by the 496.5-nm Ar^+ laser line and showing the $A_{1g}+4E_g$ and F_{2g} symmetry components, respectively.

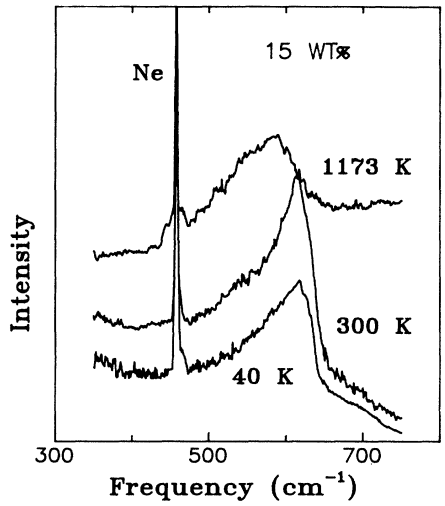

FIG. 4. $y(xy)x$ Raman spectrum of 15 wt. % YSZ excited by the 496.5-nm Ar^+ laser line at various temperatures. The sharp line is the Ne calibration line.

IV. DISCUSSION AND ANALYSIS OF DATA

A. Raman spectra of YSZ at room temperature

Our room-temperature spectra of YSZ (Figs. 2 and 3) show a definite polarization dependence and are in good overall agreement with the relevant studies of Feinberg and Perry,[5] Liu, Perry, and Ingel,[21] and Ishigame and Yoshida.[22] It has been reported[21] that fully stabilized cubic zirconia at room temperature is obtained when the yttria concentration becomes at least 15 wt. %. However, in our data the Raman scattering of the 10 wt. % concentration shows a similar spectral form with that displayed by the other two concentrations (particularly when the comparison is focused on the strong band at ~ 600 cm^{-1}). This discrepancy between previous results[21] and ours implies that the yttria content necessary for stabilization depends on the growing conditions.

The spectra of all concentrations and all symmetries are characterized by broad features indicative of the disorder existing in the oxygen sublattice after the partial substitution of Zr^{+4} by Y^{+3} cations and the consequent appearance of oxygen vacancies. In fact, the (more or less) continuum in the range 50–450 cm^{-1} appears to increase with increasing yttria content, thus reflecting the increasing disorder. Although the cation (Zr^{+4} or Y^{+3}) sublattice preserves its translational symmetry, the overall crystal generally lacks such a symmetry which results in the appearance of disorder-induced contributions to the Raman scattering from points of the Brillouin zone with $q \neq 0$ (of the ordered crystal). Therefore, mode contributions from all points of the Brillouin zone will be present in the observed spectra, in proportion to their densities of states. Feinberg and Perry[5] suggested that these spectra effectively represent the one-phonon density

TABLE I. The fitting values of the constants in Eqs. (1), (3), and (6).

	10 wt. %	15 wt. %	20 wt. %
$\omega(0)$ (cm^{-1})	615.4	617.0	605.4
a_1 (10^{-3} cm^{-1}/K)	10.5	6.42	6.40
a_2 (10^{-5} cm^{-1}/K^2)	1.13	1.39	1.57
A (10^{-2}/GPa)	−91.4	−17.4	−4.62
B (10^{-6}/GPa/K)	37.5	16.2	8.01
C (10^2 K/GPa)	223	19.2	3.11
D (10^3 K)	24.2	10.7	6.09
$B-C/D^2$ (10^{-7}/GPa/K)	−6.0	−5.7	−3.8
E (10^{-4})		1.79	
F (10^{-1} K)		6.16	
T_1 (K)		154	

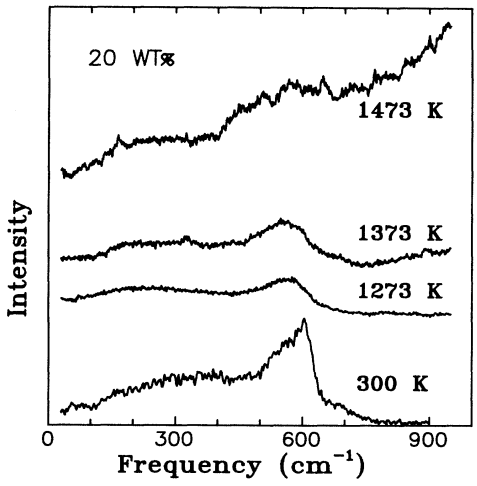

FIG. 5. $y(xy)x$ Raman spectrum of 20 wt. % YSZ excited by the 457.9-nm Ar^+ laser line at various temperatures.

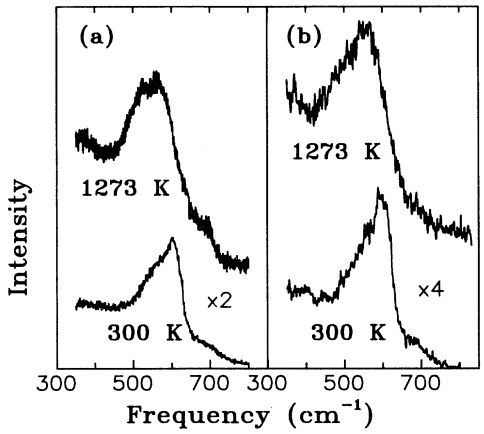

FIG. 6. Comparison of $y(xy)x$ Raman spectra of 20 wt. % YSZ at $T=300$ and 1273 K obtained without laser chopping (a) and with laser chopping (b).

of states. This argument was further supported by Ishigame and Yoshida[22] by studying the variation of intensity of the spectra observed at 300 and 2 K; they found that the intensity varies according to the $n(\omega,T)+1$ factor, where $n(\omega,T)=[\exp(\hbar\omega/kT)-1]^{-1}$ the Bose-Einstein thermal factor, thus implying first-order (one-phonon processes) rather than second-order (two-phonon processes) scattering whose intensity varies according to the product of the temperature factors of the two phonons.

The main feature of these spectra is the asymmetric band peaking at about 600 cm^{-1} which appears strongly in the cross-polarization configuration (F_{2g} symmetry). Unambiguous assignment of this band has not been made to date. The rather sharp high-frequency side of the band indicates that the main part of the band (around peak position) is owed primarily to scattering by a phonon from a critical point of the zone. By fitting this band to two

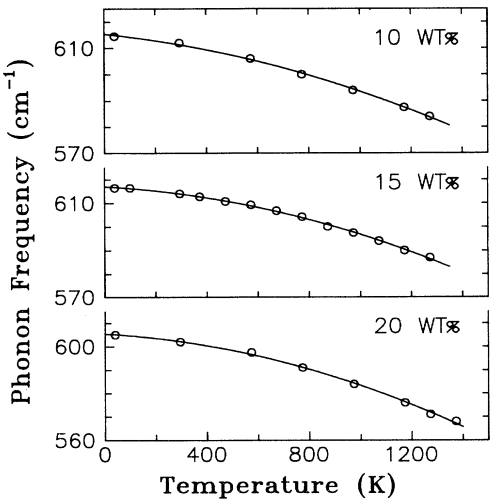

FIG. 7. Temperature dependence of the F_{2g} phonon frequency for the three YSZ compositions. The solid lines represent least-squares fits of the experimental data to Eq. (1).

Gaussian lines, we have found the half width of the central line to be 30–35 cm^{-1}. This value is much higher than the corresponding one for the zone-center F_{2g} phonon of pure fluorite-type oxides,[23,24] but in the case of YSZ such a phonon is expected to be significantly broadened given the lattice disorder and defects.

In their earlier work Feinberg and Perry[5] mentioned that they estimated a frequency of ~500 cm^{-1} for the F_{2g} zone center mode using a shell model, and concluded that the Raman peak of YSZ at 600 cm^{-1} could not be the long-wavelength optical-phonon characteristic of the fluorite-type crystals, given also its large width. In subsequent neutron-scattering experiments, the same group of researchers[25] did not observed any optical-phonon branches because of the disordering of the oxygen sublattice; however, based on the characteristics of the acoustic-phonon branches (which were observed as they are mainly due to the ordered cation sublattice), the three independent elastic constants and the observed zone-center infrared frequencies, they carried out a rigid-ion model calculation[25] which gave a frequency of 585 cm^{-1} for the F_{2g} optical phonon at the zone center. In fact the calculated dispersion curves of Liu *et al.*[25] are in good agreement with those calculated by Ishigame and Yoshida,[22] who also assumed a rigid-ion model and the peak at 600 cm^{-1} as the zone-center optical phonon.

Bearing in mind the above, we conclude that the main line at 600 cm^{-1} corresponds to the zone-center F_{2g} mode which is the only expected first-order Raman-active mode for this crystal class, and the spectra therefore consist of this Raman-active mode plus disorder-induced scattering.

B. Raman spectra at high temperatures

The spectral forms of the Raman scattering at high temperatures reflect the characteristic broadening and softening effects sustained by the various spectral features (Figs. 4–6). The F_{2g} phonon softens continuously up to the highest temperature of measurement, without any abrupt change of slope in the frequency versus temperature plots (Fig. 7). A similar softening has been observed for the satellite (broad) line at ~560 cm^{-1}. There is no evidence of a phase transition, implying that YSZ is very stable throughout the temperature range (40–1500 K).

In addition to the correlation between the spectra at 300 and 2 K through the thermal factors for first- and second-order scattering, we have extended this testing method to elevated temperatures. Using the spectrum at 300 K as reference, we have estimated the anticipated spectral forms at 973 K assuming $n+1$ (one-phonon scattering) and $(n+1)^2$ (two-phonon overtone scattering) dependences and compared them with the observed one at this temperature (Fig. 8). In these calculations, we have considered only the rates at which the intensity increases (with increasing T), as they are implied by the above thermal factors, without taking into account the shift of the peak due to anharmonic effects. The observed spectrum at 973 K lies in between the one- and two-phonon calculated spectra having an overall shape closer to that of the one-phonon spectrum. Since we have no in-

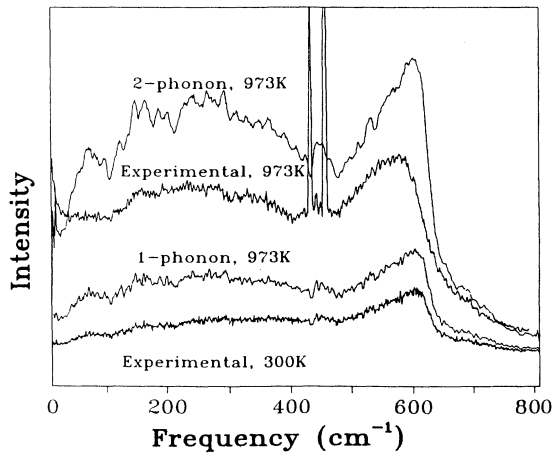

FIG. 8. Comparison between (i) observed $y(xy)x$ Raman spectrum of 15 wt. % YSZ at 973 K, and (ii) estimated spectra for this temperature assuming an $n+1$ (one-phonon scattering) or an $(n+1)^2$ (two-phonon overtone scattering) dependence and using the corresponding $y(xy)x$ Raman spectrum of this composition at 300 K as reference.

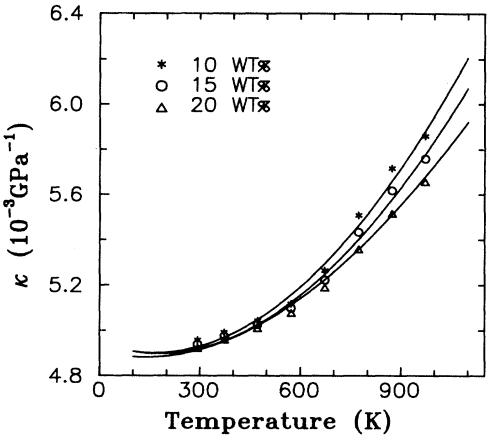

FIG. 9. Temperature dependence of the volume compressibility κ for 10, 15, and 20 wt. % YSZ crystals. The solid lines represent least-squares fits [Eq. (3)] to the extrapolated data from Ref. 26.

formation about the T dependence of the scattering cross section, we cannot be sure about the absolute intensity level and, for this reason, the comparison is only qualitative.

C. Anharmonicity analysis

In order to analyze the experimental data with the anharmonic theory, it is necessary to know the bulk compressibilities, the thermal-expansion coefficients, and the Grüneisen parameters as functions of temperature.[8–18]

1. Bulk compressibilities of cubic YSZ

For cubic crystal the volume compressibility is

$$\kappa=\frac{1}{B}=\frac{3}{C_{11}+2C_{12}}\ , \tag{2}$$

where B is the bulk modulus and C_{ij} are the components of the elastic stiffness tensor in suppressed notation. The temperature-dependent data of C_{ij} for cubic YSZ of four yttria contents for $T\geq 295$ K have been measured by Kandil, Greiner, and Smith.[26] The values, for our 10, 15, and 20 wt. % samples are obtained by extrapolation. The T dependence of the volume compressibility κ can be fitted by the following analytical form[15,18]

$$\kappa(T)=A+BT+\frac{C}{T+D}\ . \tag{3}$$

The results are shown in Fig. 9, where the solid lines represent least-squares fits of the experimental data to Eq. (3). The fitting values of constants A, B, C, and D for all three compositions are listed in Table I. It is noted that the slope of the function of Eq. (3) is $B-C/D^2$ as $T\rightarrow 0$, and these values are expected to be very small (not strictly zero, Table I) for all three yttria concentrations. Alternatively, if we require that the slope $d\kappa/dT$ becomes zero when $T\rightarrow 0$, Eq. (3) reduces to a three-parameter expression

$$\kappa(T)=A+BT+\frac{BD^2}{T+D}\ , \tag{3a}$$

which, strictly speaking, gives a more accurate fit. We have compared the results obtained by the two expressions, (3) and (3a), and found that their difference is marginal.

2. Thermal-expansion coefficients of cubic YSZ

The temperature dependence of the lattice parameter has been measured by Terblanche,[27] for five yttria contents of cubic YSZ, from RT up to 1270 K.

$$a(T)=5.1208+0.00231y+4.6468\times 10^{-5}(T-273)+7.6613\times 10^{-9}(T-273)^2\ , \tag{4}$$

where y is the Y_2O_3 content in units of mol % and T in K. The volume thermal-expansion coefficient is

$$\beta=3\alpha=\frac{3}{a(T)}\left[\frac{da(T)}{dT}\right]\ , \tag{5}$$

where α is the linear thermal-expansion coefficient. Because the correction in the Y_2O_3 compositional dependence of β is very small,[26,27] the values of $\beta(T)$ for the 15 wt. % (8.8 mol %) yttria content are chosen to describe all the 10–20 wt. % yttria compositions, with the error being less than $\pm 0.15\%$ in the temperature range 295–1270 K. To the best of our knowledge, for $T<295$ K, only Walker and Anderson[28] have measured the volume thermal-expansion coefficient for the 16 mol %

composition for $T \leq 6$ K. Assuming that the variation of $\beta(T)$ for different yttria contents of cubic YSZ at low temperatures is also small and can be neglected, the volume expansion coefficients in the whole temperature region is described by the analytical form[15,18]

$$\beta(T)=(E/T+F/T^2)\sinh^{-2}(T_1/T) . \quad (6)$$

The above form shows that β tends to zero as $T \rightarrow 0$. Figure 10 illustrates a least-squares fit to Eq. (6) with the values obtained from Eqs. (4) and (5) at $T \geq 295$ K and the experimental data for $T \leq 6$ K of Ref. 28. The fitting constants E, F, and T_1 are also listed in Table I.

It is noted that according to Refs. 15 and 18, the values of $\beta(T)$ for $T < 300$ K are calculated using the data of Debye temperature Θ_D and the expression

$$\beta(T)=\beta_\infty D(\Theta_D/T) , \quad (7)$$

where the Debye integral $D(\eta)$ is

$$D(\eta)=\frac{3}{\eta^3}\int_0^\eta \frac{x^4}{e^x-1}dx . \quad (8)$$

β_∞ is the limiting value of $\beta(T)$ at high temperatures and is equal to $\beta(300)/D(\Theta_D/300)$. We have found information for the Debye temperature of YSZ crystals only for the 8 wt. % yttria content which has the mixed structure of tetragonal and cubic phases.[29] Using this value, the results of Eqs. (7) and (8), together with the data for $T \geq 295$ K, give a rather poor fit to Eq. (6) and are shown by the full circles in Fig. 10. We ignore these values in the present computation and choose to use the results of fitting of Eq. (6), based on the data for $T \leq 6$ K, together with the data for $T \geq 295$ K.

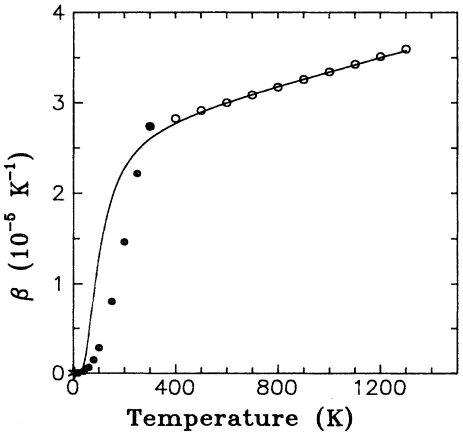

FIG. 10. Temperature dependence of the volume thermal-expansion coefficient β for cubic YSZ crystals. Open circles ($T \geq 300$ K) represent the experimental data of Ref. 27 combined with Eqs. (4) and (5). The asterisks ($T \leq 6$ K) represent the experimental data of Ref. 28. The solid line is the least-squares fit of the above points to Eq. (6). For comparison, the results of Eqs. (7) and (8) are also shown with full circles.

3. *Grüneisen parameters*

Let γ^P, γ^T, and γ^V represent the Grüneisen parameters at constant pressure, constant temperature, and constant volume, respectively. The isothermal mode Grüneisen parameter γ^T is defined by[18,30]

$$\gamma^T=-\left[\frac{\partial \ln\omega}{\partial \ln V}\right]_T=\frac{1}{\kappa\omega_0}\left[\frac{\partial\omega}{\partial P}\right]_T , \quad (9)$$

where ω_0 is the mode frequency at ambient conditions. The average values γ^T at 300 K have been determined independently from our uniaxial stress experiments[19] and are listed in Table II. The slope $(\partial\omega/\partial P)_T$ can be calculated from Eq. (9) and the values at $T=300$ K are listed in Table II.

The isobaric and isochoric mode Grüneisen parameters γ^P,γ^V, by analogy to γ^T of Eq. (9), are defined as[18]

$$\gamma^P(T)=\frac{-1}{\beta}\left[\frac{\partial \ln\omega}{\partial T}\right]_P=\frac{-1}{\beta\omega_0}\left[\frac{\partial\omega}{\partial T}\right]_P , \quad (10)$$

$$\gamma^V(T)=\frac{-1}{\beta}\left[\frac{\partial \ln\omega}{\partial T}\right]_V=\frac{-1}{\beta\omega_0}\left[\frac{\partial\omega}{\partial T}\right]_V . \quad (11)$$

According to Eq. (10), $\gamma^T(T)$ can be obtained from the slopes of the curves in Fig. 7, i.e., the derivative of Eq. (1),

$$\left[\frac{\partial\omega}{\partial T}\right]_P=a_1+2a_2T . \quad (12)$$

The constants a_1 and a_2 are listed in Table I, and $\beta(T)$ is given by Eq. (6).

Finally, the values of $\gamma^V(T)$ are taken from the

TABLE II. Bulk compressibilities, volume thermal-expansion coefficients, phonon frequencies and their pressure derivatives, temperature derivatives at constant pressure and constant volume, respectively, and Grüneisen parameters for the F_{2g} band for the three yttria concentrations at 300 K.

	10 wt. %	15 wt. %	20 wt. %
κ (TPa)$^{-1}$	4.973	4.949	4.926
β (10^{-5}/K)	2.739	2.735	2.731
ω_0 (cm^{-1})	612	614	602
$\left[\frac{\partial\omega}{\partial P}\right]_T$ (cm^{-1}/GPa)	5.79	6.08	6.52
$\left[\frac{\partial\omega}{\partial T}\right]_P$ (10^{-2} cm^{-1}/K)	−1.73	−1.48	−1.58
$\left[\frac{\partial\omega}{\partial t}\right]_V$ (10^{-2} cm^{-1}/K)	1.46	1.88	2.04
$-\beta\omega\gamma^T$ (10^{-2} cm^{-1}/K)	−3.19	−3.36	−3.62
γ^T	1.9	2.0	2.2
γ^P	1.03	0.88	0.96
γ^V	−0.87	−1.12	−1.24
η	1.84	2.27	2.29

difference $\gamma^P(T)-\gamma^T(T)$ as follows: Combining Eqs. (9)–(11), we obtain

$$\left[\frac{\partial\omega}{\partial T}\right]_P = -\frac{\beta}{\kappa}\left[\frac{\partial\omega}{\partial P}\right]_T + \left[\frac{\partial\omega}{\partial T}\right]_V \tag{13a}$$

$$= -\beta\omega_0\gamma^T + \left[\frac{\partial\omega}{\partial T}\right]_V , \tag{13b}$$

or, the alternative form

$$\gamma^P(T)=\gamma^T(T)+\gamma^V(T) . \tag{14}$$

Their values at 300 K are also included in Table II.

Notice that, in Table II, the peak frequencies ω_0, slopes $(\partial\omega/\partial T)_P$ and their relative parameters γ^P at $T=300$ K do not change monotonically with yttria concentration. A similar behavior is also displayed by the ionic diffusion coefficient,[31] that is, for low Y^{+3} contents (<9 mol. %) the carrier concentration (O^{-2}) increases as the Y^{+3} content increases, but for high Y^{+3} contents (>9 mol. %) the trends are reversed in spite of an increase in the oxygen vacancies.

D. Contributions of the volume effect and the explicit effect to the phonon frequency shifts

According to Eq. (14), the phonon frequency shifts at variable temperature under constant pressure consist of two parts: The first part is due to the volume (or implicit) effect; this reflects the change in the equilibrium interatomic spacings with temperature caused by thermal expansion. The second part is due to the pure temperature (or explicit) effect; this reflects the change in vibrational amplitudes (i.e., the phonon occupation numbers at fixed equilibrium positions).[30] The values at $T=300$ K with the corresponding terms of Eq. (13) are included in Table II.

Furthermore, the integrated form of Eq. (13a) can be expressed by

$$\Delta\omega_{\text{total}}(T)=\Delta\omega_{\text{vol}}(T)+\Delta\omega_{\text{expl}}(T) , \tag{15}$$

where the total phonon frequency shift is given by the data of Fig. 7 or the analytic form of Eq. (1),

$$\Delta\omega_{\text{total}}(T)=\omega(T)-\omega(0)=a_1T+a_2T^2 . \tag{16}$$

The shift caused by the volume thermal-expansion effect alone is given by

$$\Delta\omega_{\text{vol}}(T)=-\int_0^T\frac{\beta}{\kappa}\left[\frac{\partial\omega}{\partial P}\right]_{T'}dT' . \tag{17}$$

We assume that the variation of the slope $(\partial\omega/\partial P)_T$ is very small in the whole temperature region, i.e., $(\partial\omega/\partial P)_T$ is almost T independent. This is also the case with other materials such as Mg_2X (X=Si, Ge, Sn),[15] AlSb,[16] LaF_3.[18] The values of $(\partial\omega/\partial P)_{T'}$ obtained from the values of γ^T at $T=300$ K using Eq. (9), are listed in Table II.

By use of the analytic expressions for $\kappa(T)$ in Eq. (3) and $\beta(T)$ in Eq. (6), the calculated values of $\Delta\omega_{\text{vol}}(T)$ from Eq. (17) were obtained, and are shown by dashed lines in Fig. 11. It is shown that $\Delta\omega_{\text{vol}}(T)$ varies almost linearly with temperature in the region of $T\geq 100$ K and the absolute values of the slopes are increasing with yttria content, e.g., 3.2, 3.4, 3.6 in units of 10^{-2} cm^{-1}/K for 10, 15, and 20 wt. % Y_2O_3, respectively, at 300 K. Then, from Eq. (15),

$$\Delta\omega_{\text{expl}}(T)=\Delta\omega_{\text{total}}(T)-\Delta\omega_{\text{vol}}(T) . \tag{18}$$

The results are shown by full circles in Fig. 11 and the solid lines are to assist the eye.

It should be noted that, as shown in Fig. 11, the total downward (negative) shift of the phonon frequency $\omega(T)$ with increasing T consists of the downward (negative) shift due to the volume expansion effect and the upward (positive) shift due to anharmonicity; clearly, the volume contribution $\Delta\omega_{\text{vol}}$ prevails over anharmonicity $\Delta\omega_{\text{expl}}$ for all three yttria concentrations. This behavior is the same as for other cubic fluorite structure compounds,[14,32] such as CaF_2, SrF_2, and BaF_2, but is different from that in other materials, such as diamond, Si, Ge, ZnSe, Mg_2X (X=Si, Ge, Sr), AlSb, etc. In the latter materials both contributions $\Delta\omega_{\text{vol}}$ and $\Delta\omega_{\text{expl}}$ are of the same sign (i.e., both contribute downward shifts with increasing T).

An alternative way to determine the relative importance of the two contributions is to estimate the implicit fraction which is defined as[30,32]

$$\eta=\gamma^T/\gamma^P=\gamma^T/(\gamma^T+\gamma^V) . \tag{19a}$$

The three Grüneisen parameters $\gamma^P,\gamma^T,\gamma^V$ are defined in Eqs. (9)–(11). The values of η at $T=300$ K are calculated and listed in Table II.

Using Eqs. (9) and (10), the T dependence of the implicit fraction can be expressed by

$$\eta=-\frac{\beta(T)}{\kappa(T)}\frac{(\partial\omega/\partial P)_T}{(\partial\omega/\partial T)_P} . \tag{19b}$$

The curves of $\eta(T)$ are shown in Fig. 12. The behavior

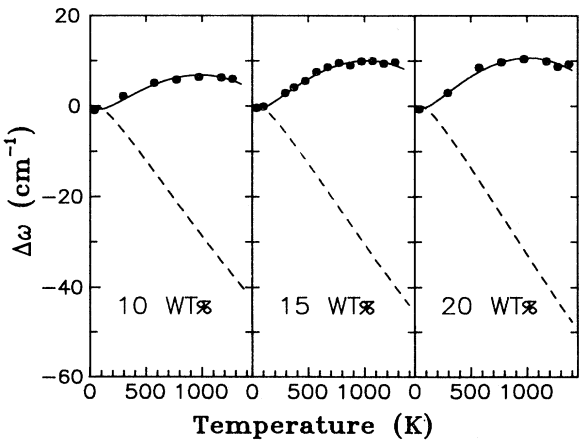

FIG. 11. Dashed lines represent the volume contribution $\Delta\omega_{\text{vol}}$ obtained from Eq. (17) and full circles represent the explicit contribution $\Delta\omega_{\text{expl}}=\Delta\omega_{\text{total}}-\Delta\omega_{\text{vol}}$. The solid lines are to assist the eye.

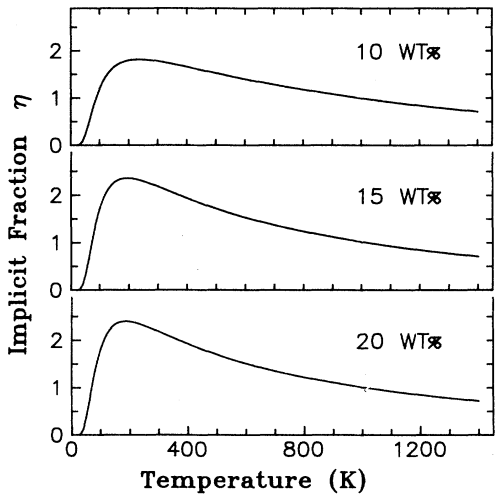

FIG. 12. Temperature dependence of the implicit fraction η according to Eq. (19b) for the three yttria concentrations.

of $\eta(T)$ is similar for the three concentrations. For $T<100$ K, $\eta(T)$ falls rapidly and approaches zero because the factor $\beta(T)$ tends to zero as $T\rightarrow 0$. At ~ 200 K, there exists a maximum which increases with increasing yttria content, i.e., 1.85, 2.36, and 2.40 for 10, 15, and 20 wt. % YSZ, respectively. For $T>250$ K, the fraction $\eta(T)$ falls slowly as the temperature increases.

It should be noted that the competition between volume and explicit effects is also shown in Fig. 12 in the various temperature regions: (i) For $T<80$ K, the explicit contribution dominates and the volume contribution diminishes. (ii) Between 80 and 100 K the fraction η remains larger than 1. From Eq. (19a), values $\eta>1$ indicate that γ^T is larger than γ^P, and γ^V is negative, i.e., the explicit effect contributes to the positive shift of the phonon frequency with increasing temperature [refer to Eq. (11)]. According to a general scheme suggested by Weinstein and Zallen,[30] values $\eta\geq 1$ imply that the bonding in cubic YSZ has ionic character and the moving ions are, in the context of the F_{2g} phonon, the oxygen anions. This behavior is similar to that of other fluorite structures,[14,32] and of LaF_3.[18] (iii) For much higher temperatures the factor η tends to 0.7 which implies that $\Delta\omega_{\rm vol}$ and $\Delta\omega_{\rm expl}$ are comparable in size and carry the same sign (both contributions tend to lower the frequency with increasing temperature). This effect can also be seen in Fig. 11.

V. CONCLUSIONS

The Raman spectra of yttria-stabilized cubic zirconia for three yttria concentrations have been studied under variable temperature over a wide range (40–1470 K). The compound is very stable throughout this range without any evidence for phase change.

The results of this work provide evidence that Raman scattering in YSZ around 600 cm^{-1} is dominated by the zone-center F_{2g} mode characteristic of the fluorite-type crystals. The broad features in the spectra have been attributed to first-order (one-phonon) processes from various critical points of the Brillouin zone activated by the crystal disorder.

The phonon frequency shifts of the F_{2g} band at variable temperatures have been measured. The total frequency shifts consist of a volume contribution and an anharmonic contribution. For the most part of the temperature region (80–1000 K) the anharmonic contribution is positive, and this indicates that the bonding of zirconia has ionic character.

ACKNOWLEDGMENTS

This work was supported in part by the General Secretariat for Research and Technology of Greece. One of us (J.C.) is grateful to the State Scholarship Foundation of Greece for financial support. Many thanks are due to C. Gemenetjis for his help in the electronics. We thank Dr. H. Schubert and Professor W. Weppner, Max Planck Institute, Stuttgart, for providing the YSZ crystals.

[1]C. M. Phillipi and K. S. Mazdiyasni, J. Am. Ceram. Soc. **54**, 254 (1971).

[2]E. Anastassakis, B. Papanicolaou, and I. M. Asher, J. Phys. Chem. Solids **36**, 667 (1975); I. Asher, B. Papanicolaou, and E. Anastassakis, J. Phys. Chem. Solids **37**, 221 (1976).

[3]M. Ishigame and T. Sakurai, J. Am. Ceram. Soc. **60**, 367 (1977).

[4]Y. K. Voron'ko, B. V. Ignat'ev, E. E. Lomonova, V. V. Osiko, and A. A. Sobol, Sov. Phys. Solid State **22**, 603 (1980).

[5]A. Feinberg and C. H. Perry, J. Phys. Chem. Solids **42**, 513 (1981).

[6]V. S. Stubican, R. C. Hink, and S. P. Ray, J. Am. Ceram. Soc. **61**, 17 (1978).

[7]E. C. Subbarao, in *Advances in Ceramics: Science and Tehcnology of Zirconia,* edited by A. H. Heuer and L. W. Hobbs (American Ceramic Society, Columbus, OH, 1981), p. 1.

[8]E. Anastassakis, H. C. Hwang, and C. H. Perry, Phys. Rev. B **4**, 2493 (1971).

[9]E. S. Zouboulis and M. Grimsditch, Phys. Rev. B **43**, 12 490 (1991).

[10]T. R. Hart, R. L. Aggarwal, and B. Lax, Phys. Rev. B **1**, 638 (1970).

[11]M. Balkanski, R. F. Wallis, and E. Haro, Phys. Rev. B **28**, 1928 (1983).

[12]J. Menendez and M. Cardona, Phys. Rev. B **29**, 2051 (1984).

[13]V. G. Khamdamov, V. I. Vettegren, and I. I. Novak, Sov. Phys. Solid State **22**, 1896 (1980).

[14]D. G. Mead and G. R. Wilkinson, J. Phys. C **10**, 1063 (1977).

[15]Y. S. Raptis, G. A. Kourouklis, E. Anastassakis, E. Haro, and M. Balkanski, J. Phys. (Paris) **48**, 239 (1987).
[16]Y. S. Raptis and E. Anastassakis, Solid State Commun. **76**, 335 (1990).
[17]F. Cerdeira, F. E. A. Mero, and V. Lemos, Phys. Rev. B **27**, 7716 (1983).
[18]E. Liarokapis, E. Anastassakis, and G. A. Kourouklis, Phys. Rev. B **32**, 8346 (1985).
[19]J. G. Cai, Y. S. Raptis, and E. Anastassakis, Appl. Phys. Lett. **62**, 2781 (1993).
[20]C. Raptis, J. Phys. E **16**, 749 (1983).
[21]D. W. Liu, C. H. Perry, and R. P. Ingel, J. Appl. Phys. **64**, 1413 (1988).
[22]M. Isigame and E. Yoshida, Solid State Ionics **23**, 211 (1987).
[23]V. G. Keramidas and W. B. White, J. Chem. Phys. **59**, 1561 (1973).
[24]M. Ishigame and M. Kojima, J. Phys. Soc. Jpn. **41**, 202 (1976).
[25]D. W. Liu, C. H. Perry, A. A. Feinberg, and R. Currat, Phys. Rev. B **36**, 9212 (1987).
[26]H. M. Kandil, J. D. Greiner, and J. F. Smith, J. Am. Ceram. **67**, 341 (1984).
[27]S. P. Terblanche, J. Appl. Crystallogr. **22**, 283 (1989).
[28]F. J. Walker and A. C. Anderson, Phys. Rev. B **29**, 5881 (1984).
[29]W. N. Lawless, Phys. Rev. B **21**, 585 (1980).
[30]B. A. Weinstein and R. Zallen, in *Topics in Applied Physics,* edited by M. Cardona and G. Guntherodt (Springer, Heidelberg, 1984), Vol. 54, p. 463.
[31]T. Suemoto and M. Ishigame, Solid State Ionics **21**, 225 (1986).
[32]G. A. Kourouklis and E. Anastassakis, Phys. Rev. B **34**, 1233 (1986).